minerals

MDPI

Article

Remobilization of HFSE, Y, and REE during Diagenetic Alteration of Heavy Minerals in Sandstones from the Chvalčov Site, Flysch Belt of the Outer Western Carpathians, Czech Republic

Zdeněk Dolníček [1], Michaela Krejčí Kotlánová [2,3], Jana Ulmanová [1] and Jiří Sejkora [1,*]

[1] Department of Mineralogy and Petrology, National Museum, Cirkusová 1740, CZ-193 00 Prague, Czech Republic; zdenek.dolnicek@nm.cz (Z.D.); jana.ulmanova@nm.cz (J.U.)
[2] Research Institute for Building Materials, Hněvkovského 30/65, CZ-617 00 Brno, Czech Republic; kotlmi@seznam.cz
[3] Institute of Geological Sciences, Masaryk University, Kotlářská 267/2, CZ-611 37 Brno, Czech Republic
* Correspondence: jiri.sejkora@nm.cz

Abstract: An in situ electron microprobe study of detrital minerals yielded important insights into the diagenetic history of the Cretaceous-to-Paleogene flysch sandstones from the Chvalčov site, Rača Unit, Flysch Belt of the Outer Western Carpathians. Detrital titanite and a Fe-Ti mineral (probably ilmenite) were almost completely altered to TiO_2 minerals, which also newly crystallized in intergranular spaces of sandstone. Brookite, anatase, and, exceptionally, rutile were identified by Raman spectroscopy. Authigenic TiO_2 phases show complex composition with occasionally elevated contents of Fe, Nb, Zr, V, Sc, Cr, Al, Y, and/or P, which were likely sourced from altered neighboring heavy minerals. In addition, rare authigenic LREE- and Y-enriched apatite rims were observed on detrital apatite. The remobilization of REE, Y, and HFSE was likely mediated by acidic early diagenetic fluids enriched in fluoride and sulfate anions. The superimposed formation of calcite cement was associated with the dissolution of detrital garnet, feldspars, and quartz. The compositions of detrital apatite and garnet ($Alm_{60-82}Prp_{4-30}Sps_{0-24}Grs_{0-19}$) are comparable with those from adjacent parts of the Flysch Belt. Detrital rutile is enriched in Nb, V, Cr, and Zr. Our study illustrates the intensity of diagenetic alteration of detrital minerals in flysch sandstones as well as the usefulness of in-situ electron-microprobe investigations for the recognition of processes influencing heavy minerals in diagenetically altered sediments.

Keywords: diagenetic alteration; heavy minerals; sandstone diagenesis; ilmenite alteration; garnet dissolution; HFSE mobility; REE mobility; TiO_2 minerals; apatite; Rača Unit

check for updates

Citation: Dolníček, Z.; Krejčí Kotlánová, M.; Ulmanová, J.; Sejkora, J. Remobilization of HFSE, Y, and REE during Diagenetic Alteration of Heavy Minerals in Sandstones from the Chvalčov Site, Flysch Belt of the Outer Western Carpathians, Czech Republic. *Minerals* **2024**, *14*, 1. https://doi.org/10.3390/min14010001

Academic Editors: Wei Tan, Xiaodong Deng, Lulu Zhao and Martin Yan Hei Li

Received: 1 November 2023
Revised: 11 December 2023
Accepted: 16 December 2023
Published: 19 December 2023

Copyright: © 2023 by the authors. Licensee MDPI, Basel, Switzerland. This article is an open access article distributed under the terms and conditions of the Creative Commons Attribution (CC BY) license (https://creativecommons.org/licenses/by/4.0/).

1. Introduction

The investigation of heavy minerals became a standard technique in petrological and provenance studies of detrital sedimentary rocks and is widely used in the geological sciences, material sciences, and archaeology. As well, the heavy minerals were frequently studied in the sandstones of the Flysch Belt of the Outer Western Carpathians. In this area, the early works dealt with the evaluation of assemblages of translucent heavy minerals, whereas the more recent papers were also focused on the determination of the chemical composition of selected provenance-specific mineral phases [1–15], namely garnet [1,2,5–7,9,12,14,15], tourmaline [5,7,9,11,13], apatite [14,15], monazite [5], amphibole [11], pyroxene [11], and chromspinels [5,7,8,10–12,14,15]. A majority of these works identified similar compositions of translucent heavy mineral assemblages in sandstones from typical flysch successions, with garnet, zircon, and rutile as main minerals, in places with more significant contents of amphibole and/or tourmaline. Accessory components are

apatite, titanite, epidote, minerals of the Al_2SiO_5 group, staurolite, and monazite. The quantitative proportions of the main heavy minerals are highly variable, with the contents of individual minerals ranging from zero to many tens of percent [3,5]. However, the possible reasons for this feature were not adequately discussed in the majority of previous works.

Most of the above-cited papers were based on routine techniques of investigation of heavy minerals, which involved the crushing of a solid sedimentary rock and the separation of a heavy mineral concentrate. Only refs. [14,15] used another methodological approach based on in situ electron microprobe investigation of heavy minerals in polished sections prepared from untreated sandstone samples. These investigations yielded textural evidence of the diagenetic alteration of many detrital mineral phases. Specifically, the diagenetic alteration of heavy minerals was not addressed in most of the above-cited regional works, except for [7,9,10,12], who reported a finely etched surface of some minerals, including garnet, tourmaline, zircon (especially metamictised), rutile, and apatite. Furthermore, refs. [14,15] showed that quartz, feldspars, garnet, apatite, and in some cases also monazite and zircon underwent variably intense diagenetic dissolution, which could be (as in case of apatite) followed by the growth of newly formed authigenic rims. In addition, refs. [14,15] reported abundant complete pseudomorphs of a TiO_2 phase after a Ti-bearing detrital phase. The only minerals that did not exhibit any signs of diagenetic alteration were muscovite and chrome spinel. The authors argued for a multi-stage alteration process likely caused by alkaline diagenetic aqueous fluids [15].

In this work, we summarize results obtained during an in situ electron microprobe study of heavy minerals present in sandstones from the Chvalčov site situated in the Rača Unit of the Flysch Belt of the Outer Western Carpathians. There are three main objectives of our study. First, we increase the limited evidence on diagenetic alteration of detrital mineral phases of flysch sandstones in the study area. Second, by means of quantitative microprobe chemical data of newly formed diagenetic phases, we confirm and further strengthen the earlier observations by [14,15] on the remobilization of otherwise usually hardly remobilizable high-field-strength elements (HFSE) and rare earth elements (REE). Third, our new data expand the still very limited compositional database of detrital heavy minerals from the Czech part of the Carpathian Flysch Belt.

2. Geological Setting

The studied site is situated in the Outer Western Carpathians, which is an external part of the Alpine-type orogenic belt of the Western Carpathians [16]. The Outer Western Carpathians consist of the Miocene molasse basin of the Carpathian Foredeep and the Upper Jurassic-to-Early Miocene fold-and-thrust Flysch Belt, representing the Tertiary accretionary wedge of the Carpathian Orogen. The Flysch Belt is formed by a sequence of tectonic slices composed of rocks of the Jurassic-to-Paleogene age. This rock series was folded and thrusted towards the NW (over the SE part of the Bohemian Massif, Figure 1) during the Alpine Orogeny in the Paleocene-Miocene. In the area adjacent to the study site, the Flysch Belt can be subdivided into the Sub-Silesian, Silesian, Fore-Magura, and Rača Units, listed from tectonic foot-wall to hanging-wall (Figure 1). The studied locality is situated in the Rača Unit, which consists mainly of Lower Cretaceous-to-Lower Oligocene rhythmically bedded marine flysch sediments [17]. In addition, sporadic isolated bodies of Jurassic-Cretaceous limestones are enclosed in flysch sequences, which represent either syn-sedimentary olistoliths or tectonically incorporated klippen [18,19]. The fluid inclusion, illite crystallinity, apatite fission track, and vitrinite reflectance data suggest that the regional diagenetic overprint of rocks in the Flysch Belt reached temperatures of up to 160–200 °C [20–22]. However, local episodic short-term production of overheated (up to 220 °C) fluids generated by tectonic processes was documented in this area [23,24].

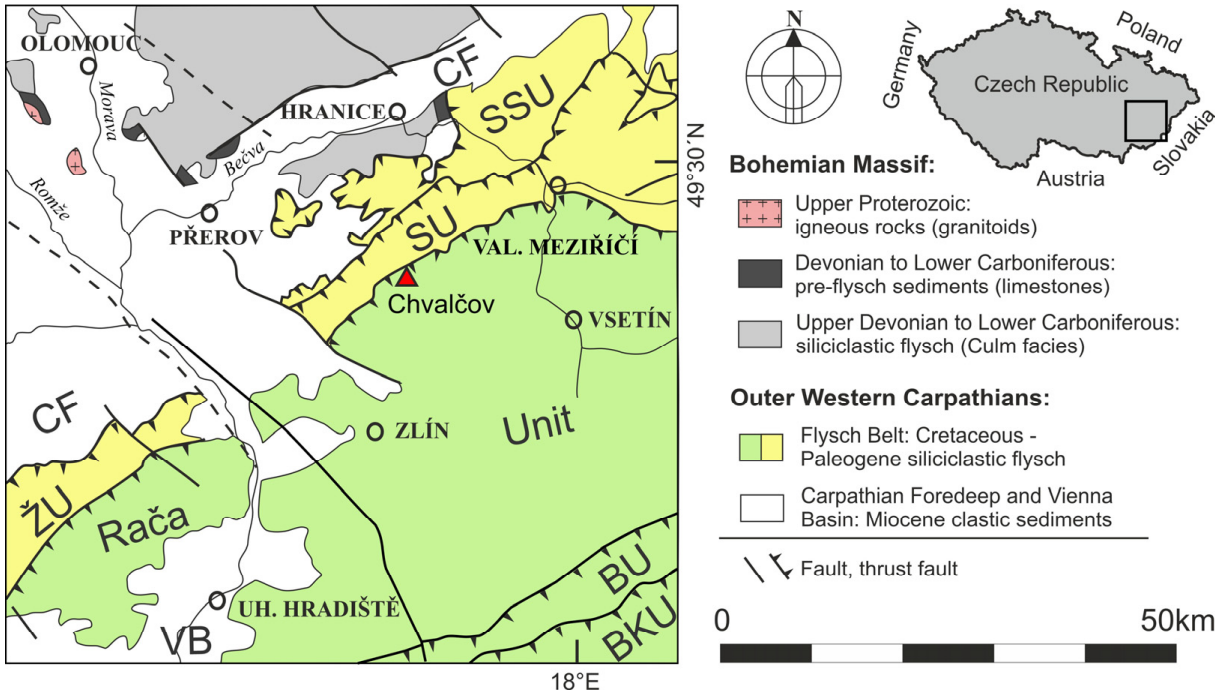

Figure 1. Geological position of the studied site (red triangle). Abbreviations: BKU—Bílé Karpaty Unit; BU—Bystrica Unit; CF—Carpathian Foredeep; SSU—Sub-Silesian Unit; SU—Silesian Unit; VB—Vienna Basin; ŽU—Ždánice Unit.

The studied site is an old quarry "Na Hrobech," situated ca. 2 km SE from the center of the village of Chvalčov and ca. 1.7 km E from the Hostýn Hill, in the Hostýn Hills, eastern Czech Republic. The quarry was mined for sandstones of the Hostýn Member of the Soláň Formation. The rocks belonging to typical sandstone-rich flysch sequences contain sandstones with arkose-to-greywacke affinity and have Upper Cretaceous-to-Paleogene age (Santonian-Eocene). The blue-grey fine- to coarse-grained sandstones alternate with grey-green claystones. These rocks are representatives of the calcareous lithofacies of the Rača Unit [17,25]. The sandstones contain a variable amount of calcareous organodetritus, together with remnants of terrestrial flora re-deposited from shallow parts of the basin. The sediments represent deep-sea turbidites deposited below the carbonate compensation depth [26].

3. Materials and Methods

The rock samples collected by one of the authors (M.K.K.) were cut by a diamond saw, and 1′ resin-mounted polished sections were prepared from suitable slabs instead of thin sections because preparation of the latter is often accompanied by pronounced damage of fine porous structures originated by diagenetic dissolution. Samples were coated by a 30 nm thick carbon film in vacuum and studied using a Cameca SX-100 electron microprobe. The textural features and mineral assemblages were documented by back-scattered electron (BSE) imaging. The individual minerals were identified by means of rapid energy-dispersive spectra (EDS). The chemical composition of selected phases was determined quantitatively by spot wavelength-dispersive (WDS) analyses. The following conditions were used for measurement of individual minerals: accelerating voltage of 15 kV, beam current of 20 nA (titanite, TiO_2 minerals, garnet) or 10 nA (apatite), and diameter of the electron beam of 0.7 μm (titanite, TiO_2 minerals), 2 μm (garnet), or 5 μm (apatite). The following elements were determined in garnet: Al, Ca, Cr, F, Fe, Mg, Mn, Na, Ni, P, Sb, Si, Sn, Ti, U, V, Y, Zn and Zr; in TiO_2 minerals: Al, As, Ca, Cr, Fe, Mg, Mn, Mo, Na, Nb, P, Pb, S, Sc, Si, Sn, Ta, U, V, W, Y and Zr; in apatite: Al, As, Ba, Ca, Ce, Cl, F, Fe, K, La, Mg, Mn, Na, Nd, P, Pb, S, Si, Sr, Y and Zn; and in titanite: Al, Ca, Ce, F, Fe, Hf, La,

Mg, Mn, Na, Nb, Nd, P, Pb, Pr, Sc, Si, Sn, Ta, Ti, Y and Zr. The following standards and wavelengths were used: albite (NaKα), almandine (AlKα, FeKα), antimonite (SbLα), apatite (CaKα, PKα), baryte (BaLα), celestine (SKα, SrLβ), $CePO_4$ (CeLα), clinoclase (AsLα), Cr_2O_3 (CrKα), $CrTa_2O_6$ (TaLα), diopside (MgKα), halite (ClKα), hematite (FeKα), Hf (HfMα), $LaPO_4$ (LaLα), LiF (FKα), Nb (NbLα), $NdPO_4$ (NdLβ), Ni (NiKα), $PrPO_4$ (PrLβ), rhodonite (MnKα), sanidine (KKα, SiKα, AlKα), $ScVO_4$ (ScKα), scheelite (WLα), Sn (SnLα), TiO_2 (TiKα), UO_2 (UMα), V (VKα), vanadinite (PbMα), wollastonite (CaKα, SiKα), wulfenite (MoLα), YVO_4 (YLα), zincite (ZnKα), and zircon (ZrLα). The peak counting times were usually between 10 and 30 s; those of both backgrounds were half of the peak time. The raw counts were converted to wt.% using a standard PAP correction matrix [27]. Oxygen was calculated from stoichiometry. The data were automatically corrected for overlaps: Cr vs. V, Mn vs. Cr, P vs. Ca, Zr vs. P, Zr vs. Nb, Hf vs. Ti, and Y vs. Nb. The contents of the above-specified elements, which are not given in tables of mineral analyses (attached as an electronic Supplementary File), were in all cases below detection limits, which mostly ranged between 0.03 and 0.09 wt.%. For La, Nd, Pr, Ta, W, Sr, and F, the detection limits were between 0.1 and 0.2 wt.%.

The Raman spectra of TiO_2 polymorphs were collected in the range 50–3500 cm^{-1} using a DXR dispersive Raman Spectrometer (Thermo Scientific) mounted on a confocal Olympus microscope in National Museum in Prague. The Raman signal was excited by an unpolarized green 532 nm solid-state diode-pumped laser and detected by a CCD detector. The instrument was set up by a software-controlled calibration procedure using multiple emission lines of neon (wavelength calibration), multiple Raman bands of polystyrene (laser frequency calibration), and standardized white-light sources (intensity calibration). The used experimental parameters were: 100 × objective, 10 s exposure time, 10 exposures, 50 μm pinhole spectrograph aperture, and 8 mW laser power level. The eventual thermal damage of the measured point was excluded by visual inspection of the excited surface after measurement, observation of possible decay of spectral features at the start of excitation, and checking for thermal downshift of Raman lines. Spectral manipulations were performed using the Omnic 9 software (Thermo Scientific). The obtained spectra were automatically compared with reference spectra of minerals from the RRUFF database.

4. Results

4.1. Sandstone Petrography

The studied rocks are gray, medium-grained sandstones. The psammitic detrital material is well sorted; the clasts with sizes between ca. 200 and 600 μm prevail, whereas coarsely clastic (>700 μm) material is rare and a clayey-silty matrix is missing (Figure 2a–f). Quartz is the main detrital phase in sandstones and is followed by K-feldspar (often perthitic; Figure 2b), plagioclase (with compositions ranging from albite to oligoclase; Figure 2a–c), and rock fragments (phyllite, limestone, and a clayey-silty sediment; Figure 2f). Micas are represented by muscovite and biotite (sometimes slightly chloritized; Figure 2a). Accessories are garnet, apatite, zircon, TiO_2 minerals, titanite, monazite, baryte, pyrite, and from the latter formed limonite. In addition, glauconite and phosphorite pellets (Figure 2f), as well as fragments of calcareous fossils, were observed sporadically.

The rock cement is exclusively formed by calcite (Figure 2). Its quantity varies widely among samples as well as within a single sample. In clast-dominated portions of the rock, the cement takes only around 20 vol. % and fills the remaining free space among densely arranged detrital grains, which in some places show signs of pressure dissolution on mutual contacts (Figure 2b). In contrast, in some portions of the rock, the cement has basal character, taking up to 70 vol. % (Figure 2d). In both cases, corrosion of clasts by the cement is evident (Figure 2a–f). Calcite cement is sometimes compositionally heterogeneous in BSE images, showing a poly-phase nature (an indistinct growth zonation and/or abundant hair-thin veinlets cutting both clasts and earlier cement are observed at higher beam currents in BSE). Such zonation is attributed to various amounts of isomorphic elements (e.g., Fe, Mg, and Mn) bound in the crystal structure of calcite. No mineral inclusions are usually observed in

calcite cement; its purity is also confirmed by EDS spectra, which lack peaks of Al and/or Si. This suggests the absence of a finely dispersed clayey fraction in the cement.

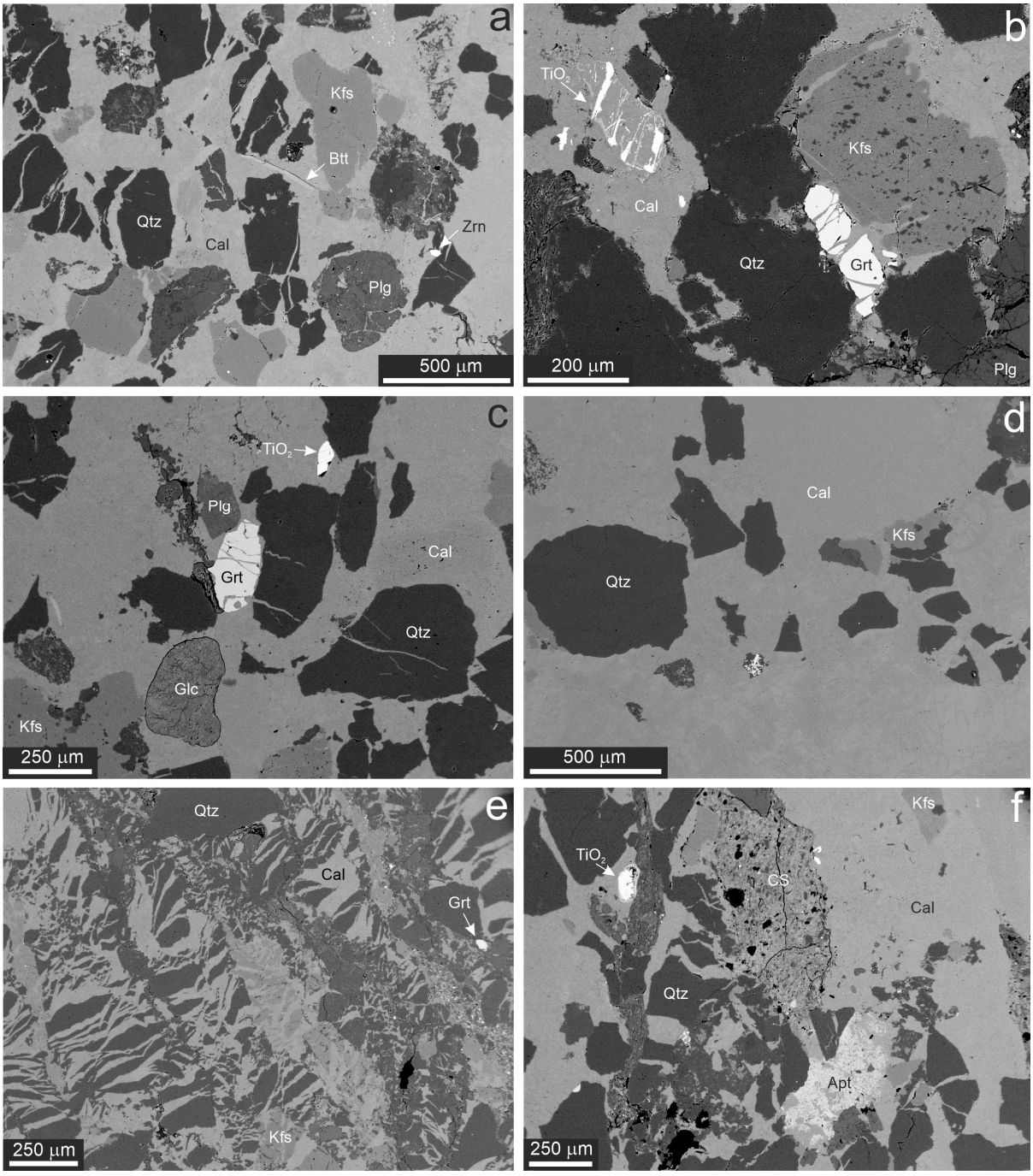

Figure 2. Fabric of the studied sandstone on BSE images. (**a**) Corroded psammitic clasts enclosed in calcite cement. (**b**) A detailed view of tightly packed corroded clasts of quartz, perthitic K-felspar, garnet, and T2b TiO_2 phase (determined as brookite). (**c**) Siliciclastic detritus (including a grain of detrital T1 TiO_2 phase) and a pellet of glauconite hosted by basal calcite cement. (**d**) A portion of rock dominated by calcite cement. (**e**) A strongly fractured portion of rock with numerous calcite veinlets cutting several neighboring clasts. (**f**) Apatite III (phosphorite) aggregate and a clast of silty claystone (CS), both strongly corroded by calcite cement, and a TiO_2 phase belonging to T2b type. Mineral abbreviations: Apt—apatite; Btt—biotite; Cal—calcite; Glc—glauconite; Grt—garnet; Kfs—K-feldspar; Plg—acid plagioclase; Qtz—quartz; Zrn—zircon.

Most siliciclastic grains—quartz, feldspars, clayey sediment, and many grains of accessory minerals (garnet, apatite, monazite, titanite, and a Fe-Ti mineral)—show signs of intensive corrosion (Figure 2a–f). Therefore, it is often not possible to assess their original size and shape. The dissolution of grain margins is indicated by teeth- or saw-shaped grain outlines as well as deep embayments fulfilled by calcite cement (Figure 2a–d) [28–30]. In addition, the dissolution processes operated also along cracks in mineral grains (Figure 2a,b), which is indicated by complexly shaped fractures with unmatching walls (contrary to fractures with matching walls), which originated due to the mechanical opening of a fracture without significant dissolution of the host mineral [31,32]. The free space created by dissolution was mostly filled by calcite cement. Part of the observed calcite veinlets undoubtedly originated during late tectonic episodes in well-cemented rock, as is suggested by systems of subparallel veinlets cutting several neighboring clasts (Figure 2e). Both diagenetic dissolution and younger fracturing gave rise to the typical textures observed in the studied sandstones, which are formed by a group of several sub-grains (relics) formed at the expense of a single original clast. These relics usually have sizes in the range of several μm to tens of μm and are mutually separated by variously thick calcite infills (Figure 2a,e). The intensity of dissolution could be very high, with an estimated volume of dissolved material commonly in the range of tens of vol. %, with maxima around 50 vol. %. In some domains, especially where quartz grains were intensely dissolved, the amount of preserved detrital material can be even lower than that of calcite cement (Figure 2c,d,f). Such calcite-dominated domains are irregularly shaped, with gradual transitions into adjacent clast-richer portions of the rock.

A smaller part of clasts (including quartz and feldspars) does not exhibit any signs of dissolution. However, as already mentioned by [14,15], the electron microscopy of polished sections is not a suitable method for the identification of weak dissolution, which is often restricted to the mineral surface only [33,34]. Muscovite, biotite, glauconite, and detrital TiO_2 minerals seem to display no features of dissolution in the material under this study (Figures 2c and 3a,b).

In summary, the studied rock can petrographically be described as a medium-grained, well-sorted quartz sandstone (or possibly arkosic sandstone; the quantification of main detrital compounds was not conducted) with corrosive pore-to-basal calcite cement and a lack of silty-clayey matrix. Parts showing a pronounced degree of replacement of clasts by cement, and thus characterized by a predominance of calcite, petrographically correspond to sandy limestone.

4.2. Characterization of Selected Heavy Minerals

The detailed attention was paid to some accessory minerals, which belong to the heavy mineral fraction, namely TiO_2-group minerals, garnet, apatite, zircon, and monazite. The electron-microprobe study of chemical composition was performed for garnet, apatite, and TiO_2-group minerals. Full data sets of collected compositions are included in an electronic Supplementary File.

The **TiO_2-group minerals** are far more frequent heavy minerals. Three principal types occur. The first one (denoted as T1 in the following text) includes anhedral to idiomorphic compositionally homogeneous non-porous detrital grains (Figure 3a,b). Raman spectroscopy identified this mineral invariably as rutile.

The second type (T2) comprises polycrystalline aggregates with variable porosity, which were formed by the replacement of clasts from earlier Ti-bearing mineral phases. In this case, two subtypes can be distinguished. The first one (T2a) is relatively rare (three cases recorded) and includes pseudomorphs containing a relatively low amount (ca. 30 vol. %) of well-defined "coarse-crystalline" (with grain size in the range of tens of μm) xenomorphic grains of a TiO_2 phase, which are associated with common calcite matrix and sparse corroded relics of titanite. Raman spectroscopy identified predominating anatase and minor brookite, both forming individual grains even within a single pseudomorph (Figure 3c). The second subtype (T2b) is much more frequent (32 items recorded) and shows

highly variable textures and compositions (Figure 3d–m). In this case, the TiO_2 phase is largely associated with Fe-(hydro)oxides and calcite, less frequently only with calcite. The outline of the original detrital mineral grain is often highlighted with a thin rim composed of a mixture of Fe-Ti oxides (Figure 3d,f,g). The internal parts of former mineral clasts show variable textures, from fine-grained, finely porous aggregates of Fe-Ti oxides with rather uniform composition (Figure 3d) to variously textured mixtures of calcite and larger (tens of μm) xenomorphic grains or (hyp)automorphic elongated or isometric crystals of a Ti-oxide (Figure 3e–l), the latter often with small in BSE image brighter particles richer in Fe (Figure 3f). The TiO_2 phase takes largely between ca. 20 and 80 vol. % of the former clast. In a few cases, features of complete dissolution of parts of the original detrital grains of Ti-minerals were recorded, which are usually indicated by a gradual decrease in the contents of the TiO_2 phase towards the margin of the former detrital grain (Figure 3m,n). Raman analyses of TiO_2 phases yielded various results with respect to texture: Fine-grained Fe-rich portions (Figure 3d,e) gave only fluorescence; well-defined elongated individuals and xenomorphic isometric grains (Figure 3e) belong to brookite; and well-defined isometric euhedral crystals (Figure 3e,k) are largely anatase and exceptionally rutile. In the latter case, both minerals seem to form fine intergrowths with grain sizes below ca. 1 μm, yielding combined Raman spectra in each spot.

The last type (T3) is a newly formed TiO_2 phase, which grows over surrounding clasts of quartz and occurs in proximity of the above-characterized deeply altered grains of earlier Ti-minerals (type T2). The elongated laths, often fan-arranged, characterize the development of the T3 TiO_2 phase (Figure 3o,p). Raman analysis identified this mineral as brookite.

A detailed microprobe study showed some differences and similarities in the composition of the above-characterized textural types of the TiO_2 minerals in the studied samples. However, the compositions of co-existing individual TiO_2 polymorphs do not differ mutually, making them, in turn, indistinguishable in BSE images. Therefore, we present compositional data on the basis of textural types (Figure 4) and not according to mineral identity.

The detrital rutile (T1) showed the highest contents of Cr (0.002–0.004 apfu), the lowest contents of Ca (≤0.002 apfu) and Fe (≤0.004 apfu), the contents of Al, P, and Si below detection limits, the best analytical totals (99+ wt%), and the best stoichiometry of the empirical formula (sum of cations ranges between 1.001 and 1.003 apfu; apfu values are based on 2 atoms of oxygen) of the whole dataset. The contents of Nb (0.001–0.006 apfu) and V (0.003–0.007 apfu) are, on average, higher than in other recognized types of TiO_2 phases. The Zr contents are comparable to those of other types of TiO_2 phase (0.001–0.004 apfu).

Both other textural types of TiO_2 phase (T2, T3) show largely much higher Ca contents (0.001–0.030 apfu), much poor stoichiometry (sum of cations ranges 1.001–1.121 apfu even considering all Fe as Fe^{3+}), and mostly also low analytical totals (89–99 wt%). The contents of Fe, Nb, Zr, and V were recorded in most collected analyses but in highly variable concentrations (0.001–0.386 apfu Fe, ≤0.006 apfu Nb, ≤0.007 apfu Zr, ≤0.011 apfu V). In addition, the contents of Si (≤0.065 apfu), Al (≤0.041 apfu), and P (≤0.006 apfu) are often elevated; rarely, Mn (≤0.020 apfu), Mg (≤0.004 apfu), Sc (≤0.004 apfu), Y (≤0.003 apfu), Cr (≤0.003 apfu), Pb (≤0.001 apfu), and/or S (≤0.001 apfu) were also detected. The wide compositional differences are mostly observed among different original clasts; however, high chemical heterogeneity may also characterize various places within a single clast, even in cases formed by a single TiO_2 polymorph. No simple correlations exist among the contents of different elements in the studied TiO_2 phases (Figure 4). On average, the T2a and T3 subtypes show markedly lower Fe contents (both ≤0.023 apfu) than the T2b one (often above 0.020 apfu).

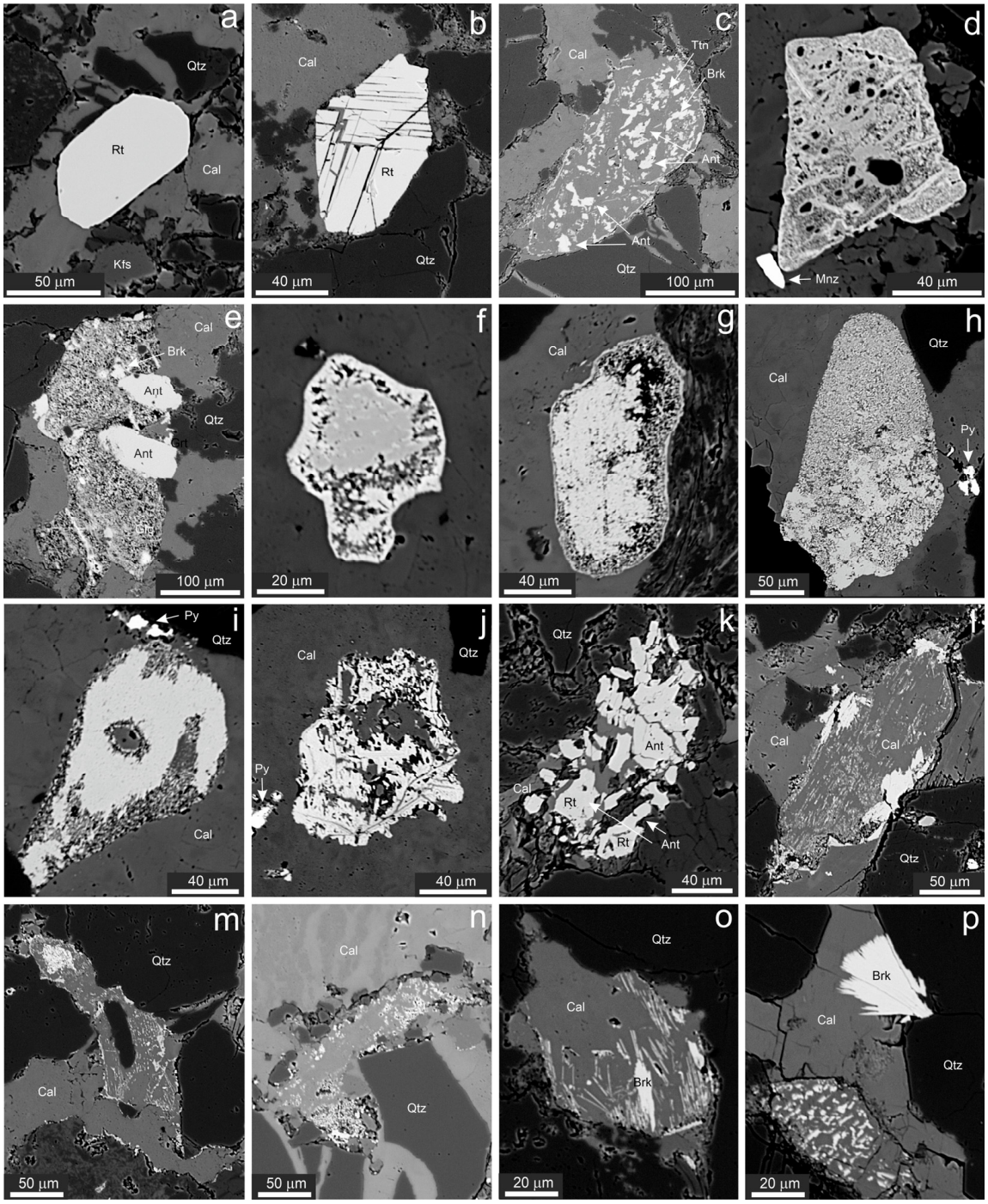

Figure 3. Examples of textural varieties of TiO_2-group minerals from the studied sandstone are shown on BSE images. In a single picture, the Fe-richer portions are brighter than the Ti-richer ones. Where Raman identification was performed, the exact mineral identification is given. (**a**,**b**) The T1-type TiO_2 phase (detrital rutile). (**c**) The T2a-type TiO_2 phase (in a pseudomorph after titanite). (**d**–**k**) The T2b-type TiO_2 phase (in pseudomorphs, probably after ilmenite). (**l**–**o**) Former clasts show a pronounced dissolution with only a small amount of preserved TiO_2 phase. (**p**) The T3-type TiO_2 phase (authigenic fan of brookite) is grown on detrital quartz in the upper part of the picture. Mineral abbreviations: Ant—anatase; Brk—brookite; Mnz—monazite; Py—pyrite; Rt—rutile; Ttn—titanite; for others, see the caption of Figure 2.

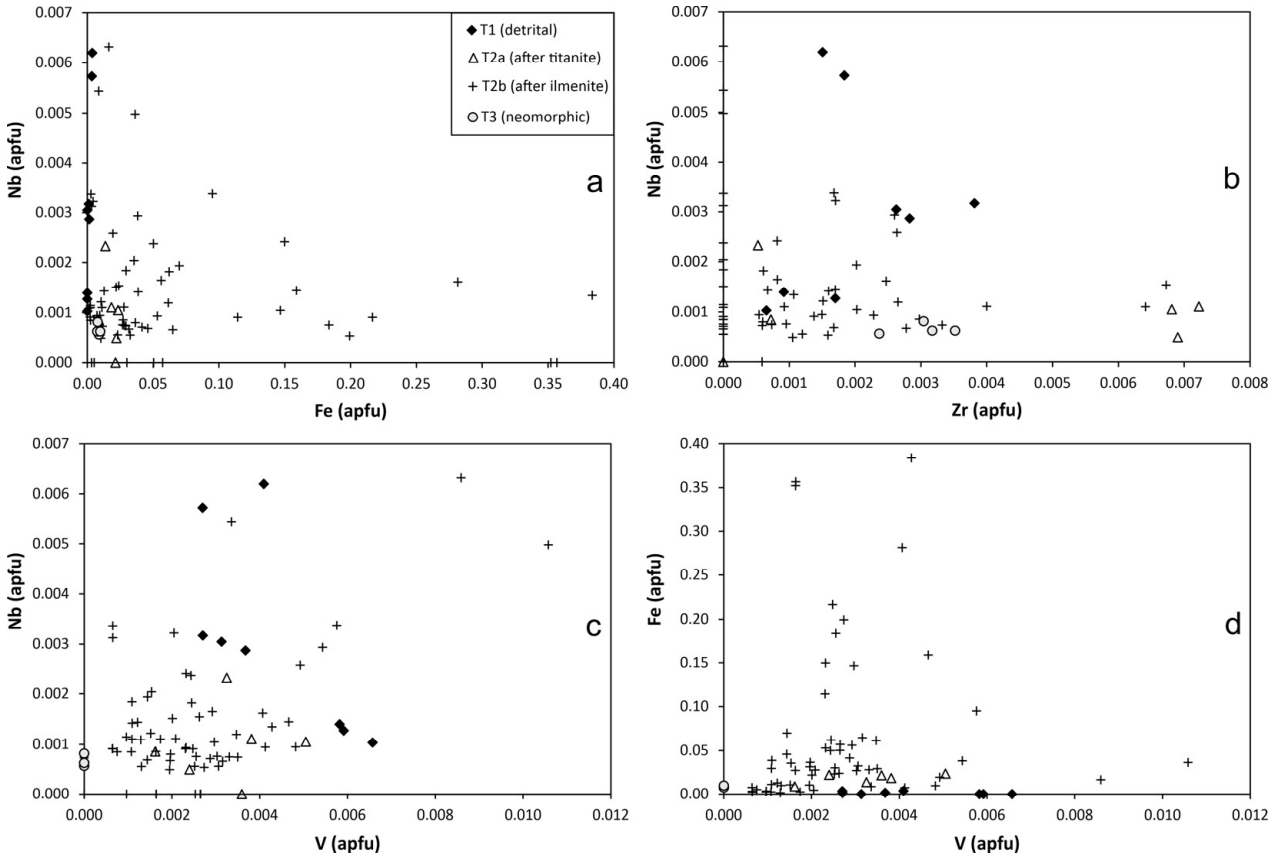

Figure 4. Variations in contents of Fe, Nb, Zr, and V in TiO_2 phases from Chvalčov. (**a**) The Fe vs. Nb plot. (**b**) The Zr vs. Nb plot. (**c**) The V vs. Nb plot. (**d**) The V vs. Fe plot.

Relics of titanite associated with the T2a TiO_2 phase (Figure 3c) show minor admixtures of Al (0.057 and 0.064 apfu), F (0.047 and 0.051 apfu), Zr (0.001 and 0.003 apfu), and Fe (0.010 apfu).

Garnet represents the second most frequent heavy mineral in the studied sandstones (27 grains were recorded). Its clasts are always slightly (Figure 5a–c) to strongly (Figure 5d–f) corroded by calcite cement. The corrosion is manifested by the saw-like outline of the grains (Figure 5b,c), as well as by groups of small relics distributed within the whole space of the original clast (Figure 5d–f). Individual relics are always mutually separated by a layer of calcite cement. No zonality of garnet grains was observed in BSE images. Quartz, biotite, chlorite, or rutile inclusions were found to be exceptionally enclosed in garnet grains (Figure 5a–c); these inclusions are sometimes sticking out from the garnet grain (Figure 5c), further manifesting an extensive dissolution of the original garnet surface. The chemical composition of garnets was studied in detail; two spot analyses were collected from each clast in order to check possible zonality. The studied garnets are always almandines with elevated pyrope, spessartine, and/or grossular components and negligible amounts of other compounds ($Alm_{60-82}Prp_{4-30}Sps_{0-24}Grs_{0-19}And_{0-1}Mzr_{0-1}Uvr_{<0.3}TiGrs_{<0.3}Glm_{<0.3}$). A minimum zonality of garnet grains is obvious, as the differences in contents of individual garnet components are usually below 1 mol. % (a maximum as high as 2.8 mol. % was recorded in one garnet grain). The subordinate garnet components show a large spread of abundances without apparent mutual correlations. Our observations did not confirm that garnets with similar compositions would exhibit a similar level of corrosion.

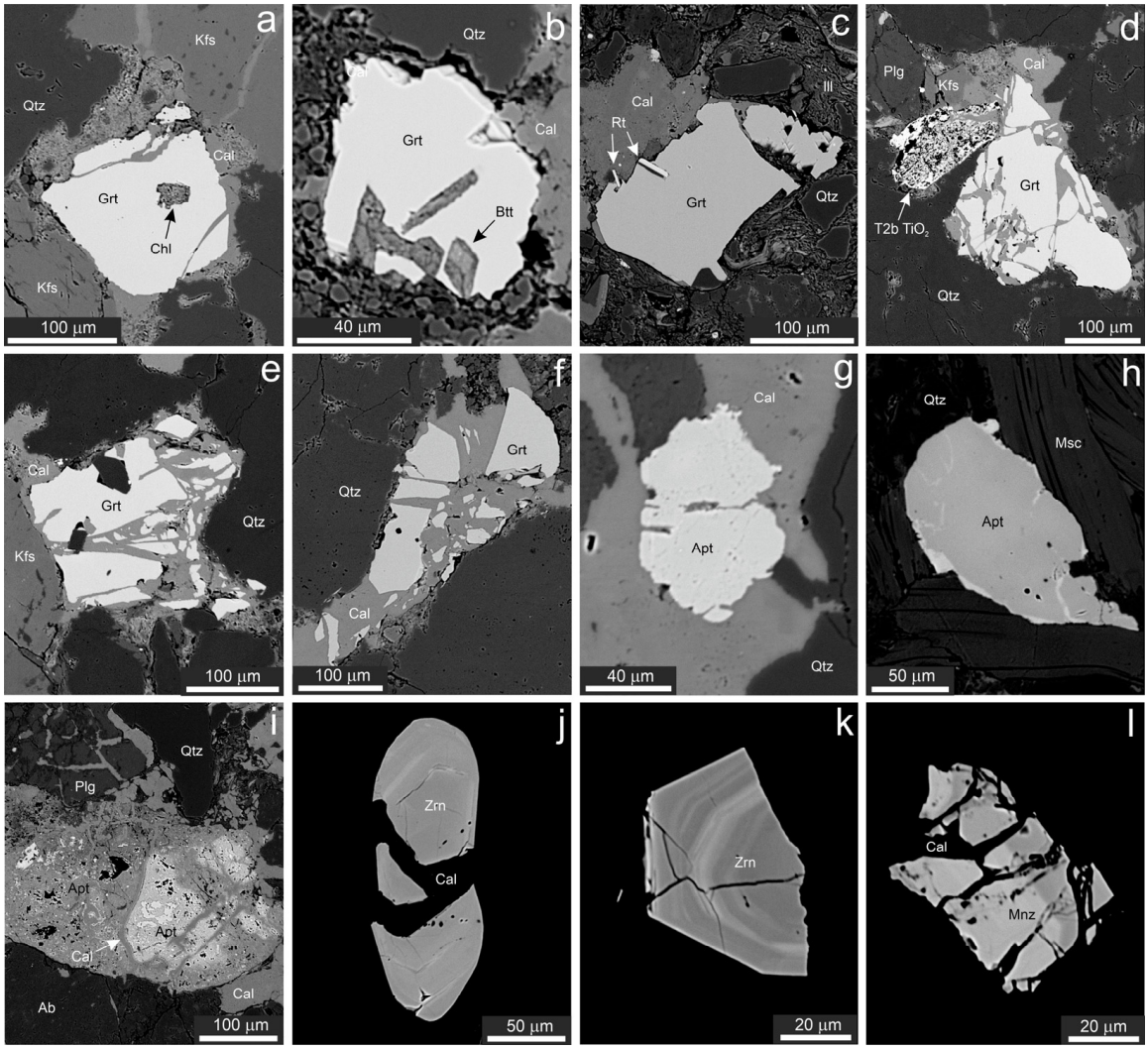

Figure 5. The nature of detrital grains of garnet, apatite, zircon, and monazite from the studied sandstone on BSE images. (**a**–**c**) Garnet grains show signs of dissolution, mainly on the outer surface. (**d**–**f**) Garnet grains showing intense dissolution along internal fractures. (**g**) Detrital apatite with a corroded surface. (**h**) Apatite with authigenic REE,Y-enriched rim (brighter hue). (**i**) an irregularly zoned phosphorite nodule containing three compositional varieties of apatite and minor calcite. (**j**) Oval zircon cut by calcite veinlets with matching walls. (**k**) Zoned euhedral zircon with weak signs of corrosion on a single original crystal face. (**l**) Slightly zoned monazite with marks of dissolution along cracks filled out by calcite. Mineral abbreviations: Ab—albite; Chl—chlorite; Ill—illite; Msc—muscovite; for others; see captions in Figures 2 and 3.

Three textural and compositional types were distinguished among the eleven found **apatite** grains. Type I represents detrital abiogenic apatite, which forms isometric homogeneous grains often with signs of corrosion that occurred at their surface or along cracks (Figure 5g). No zonality is observed in BSE images. Chemical composition corresponds to stoichiometric fluorapatite (3.00–3.03 apfu of elements in the structural position of phosphorus; basis of recalculation: 5 apfu of elements in the position of Ca) with good analytical totals (100 ± 1.5 wt%). The F contents vary between 0.64 and 1.36 apfu; the higher values than the theoretic amount of 1.00 apfu can be the result of easy diffusion of F in unsuitably oriented crystals with respect to incidental electron beam [35]. In some cases, elevated contents of Fe (≤0.040 apfu), Mn (≤0.025 apfu), LREE (≤0.015 apfu Ce), and Cl (≤0.040 apfu) were found.

Type II is a newly formed apatite that grows over one corroded clast of fluorapatite and fills up tiny veinlets in it. It is markedly different in the BSE image due to a brighter hue (Figure 5h). The chemical composition is characterized by a slight deficit of elements in the position of phosphorus (0.036–0.052 pfu), suggesting the presence of a small amount of CO_2. Slightly lower analytical totals (~98 wt%) likely suggest an increased porosity of this apatite. In addition, high F (above 1 apfu), elevated contents of alkalis (0.037–0.098 apfu Na+K), LREE (0.080–0.102 apfu La+Ce+Nd), and Y (0.022–0.030 apfu) were recorded.

Type III apatite is represented by two small nodules of phosphorite, reaching a size in the range of hundreds of μm. One has a rounded outline, whereas the other is strongly corroded by calcite cement from the margins (Figure 2f). The larger one exhibits heterogeneous internal fabric in BSE, with three variously bright apatite varieties (the brightest in the core and the darkest in the margins) and minor calcite rimming the brighter core of the nodule (Figure 5i). The chemical composition of this apatite is characterized by high F (always above 1 apfu), a deficit of elements in the position of P, suggesting elevated contents of C (0.11–0.43 apfu), and elevated contents of alkalis (0.03–0.17 apfu Na+K). Whereas the in BSE brightest oldest parts of nodule have analytical totals close to 100 wt% and lack of Si, S, Fe, and LREE, both two younger and in BSE darker compositional varieties exhibited low analytical totals (79–98 wt%) and elevated contents of S (0.010–0.051 apfu), Fe (0.01–0.12 apfu), LREE (0.008–0.047 apfu La+Ce+Nd), and in most cases also Si ($\leq$0.54 apfu).

Eleven grains of **zircon** were recorded, which exhibit either an idiomorphic habit or an oval shape. Some of them show cracks filled up by calcite veinlets with matching walls (Figure 5j), i.e., without signs of more intense dissolution. Shallow dissolution pits are exceptionally observed only at the outer surface of some grains (Figure 5k). The studied zircons are homogeneous or distinctly zoned in BSE images (Figure 5k). The EDS spectra indicate small common admixtures of Hf, in places also U, Al, and/or Ca.

Monazite is rare; we found only two grains reaching up to 90 μm in size, in both cases moderately corroded. A number of fragments formed at the expense of the original monazite grain are preserved, with sizes up to 20 μm, cemented by calcite (Figure 5l). Weak zonality of monazite is observed in BSE images, defined by admixtures of Th and Ca. Cerium is the predominating REE in both monazites, according to EDS spectra.

5. Discussion

5.1. Regional Comparison of Chemical Composition of the Minerals

Prior to discussing the mechanism of diagenetic alteration of heavy minerals, it would be useful to compare the compositions of individual minerals observed in our samples with those from adjacent Carpathian flysch sequences in order to test whether the studied samples represent some local compositional anomaly or not. However, this can only be carried out for garnet and apatite and not for detrital rutile, for which no compositional data are published.

The chemical composition of detrital garnet from Chvalčov is characterized by dominating almandine with subordinate pyrope, grossular, and/or spessartine components, with rather wide variations in the contents of these minor garnet compounds. According to literary data, such petromict ranges of garnet composition are widespread in the sandstones of the neighboring portions of the Carpathian Flysch Belt (Figure 6).

The first electron-microprobe data on detrital apatite from the Flysch Belt reported in this work and ref. [15] suggest that it belongs to fluorapatite with a stoichiometric Ca:P ratio. The observed differences in the contents of LREE, S, Cl, Fe, and Mn imply the potential usefulness of electron-microprobe data in this respective area (cf. [36]).

Phosphorite micronodules are interpreted as intraclasts initially precipitated in shallower parts of the basin and then re-deposited in the deeper parts of the basin together with other siliciclastic material [37]. The composition of phosphorites from Chvalčov is comparable to those of much larger (up to several cm-sized) phosphorite nodules in places occurring in the sedimentary sequences of the Flysch Belt, having carbonate-fluorapatite compositions with often elevated Na, LREE, Si, Al, and/or S (Figure 7) and low analyt-

ical totals. The latter is likely due to the fine porosity generated during its formation. Some authors argue for a stepwise mechanism of abiogenic crystallization of authigenic apatite in sedimentary basins, beginning with the precipitation of an unstable hydrated gel of calcium phosphate, which is subsequently slowly transformed into stable anhydrous carbonate-fluorapatite due to the addition of fluoride and carbonate anions from pore fluids [38–40]. Dehydration of the initial gel may thus give rise to the fine porosity of the final carbonate-fluorapatite.

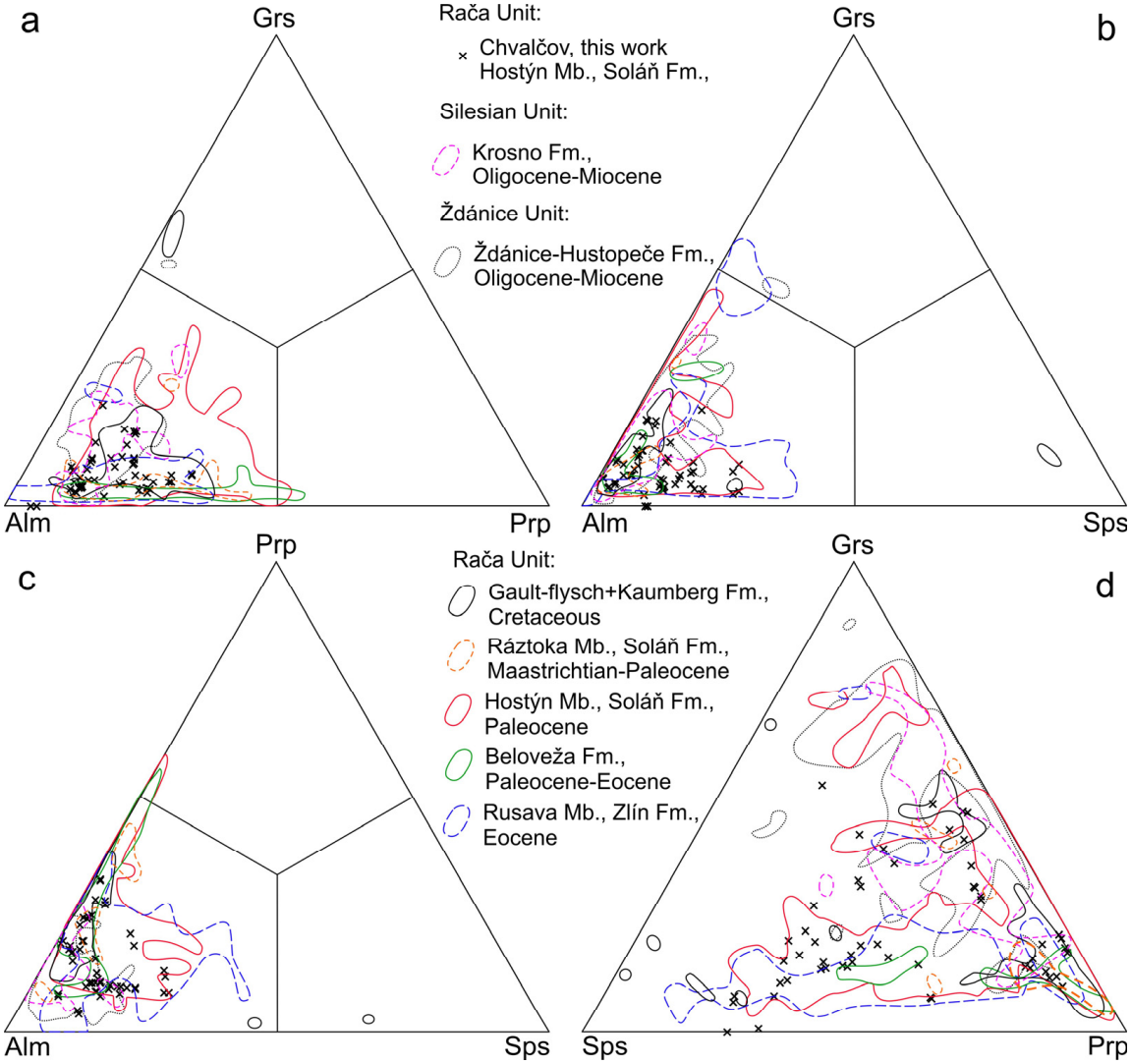

Figure 6. Variations in the chemical composition of detrital garnet from Chvalčov and comparison with published data from neighboring portions of the Carpathian Flysch Belt. (**a**) Plot almandine–grossular–pyrope. (**b**) Plot almandine–grossular–spessartine. (**c**) Plot almandine–spessartine–pyrope. (**d**) Plot spessartine–grossular–pyrope. Comparative data are taken from [1,2,6,14,15].

The rarely recorded overgrowths on detrital apatite (Type II apatite) show similar compositional trends as phosphorite micronodules (Figure 7), linking to their in situ (intrabasinal) origin.

It can be concluded that the compositions of garnet and apatite from the studied site are well comparable with those from the adjacent parts of the Flysch Belt. Therefore, the studied samples represent typical detrital phases of the area and not a local compositional anomaly.

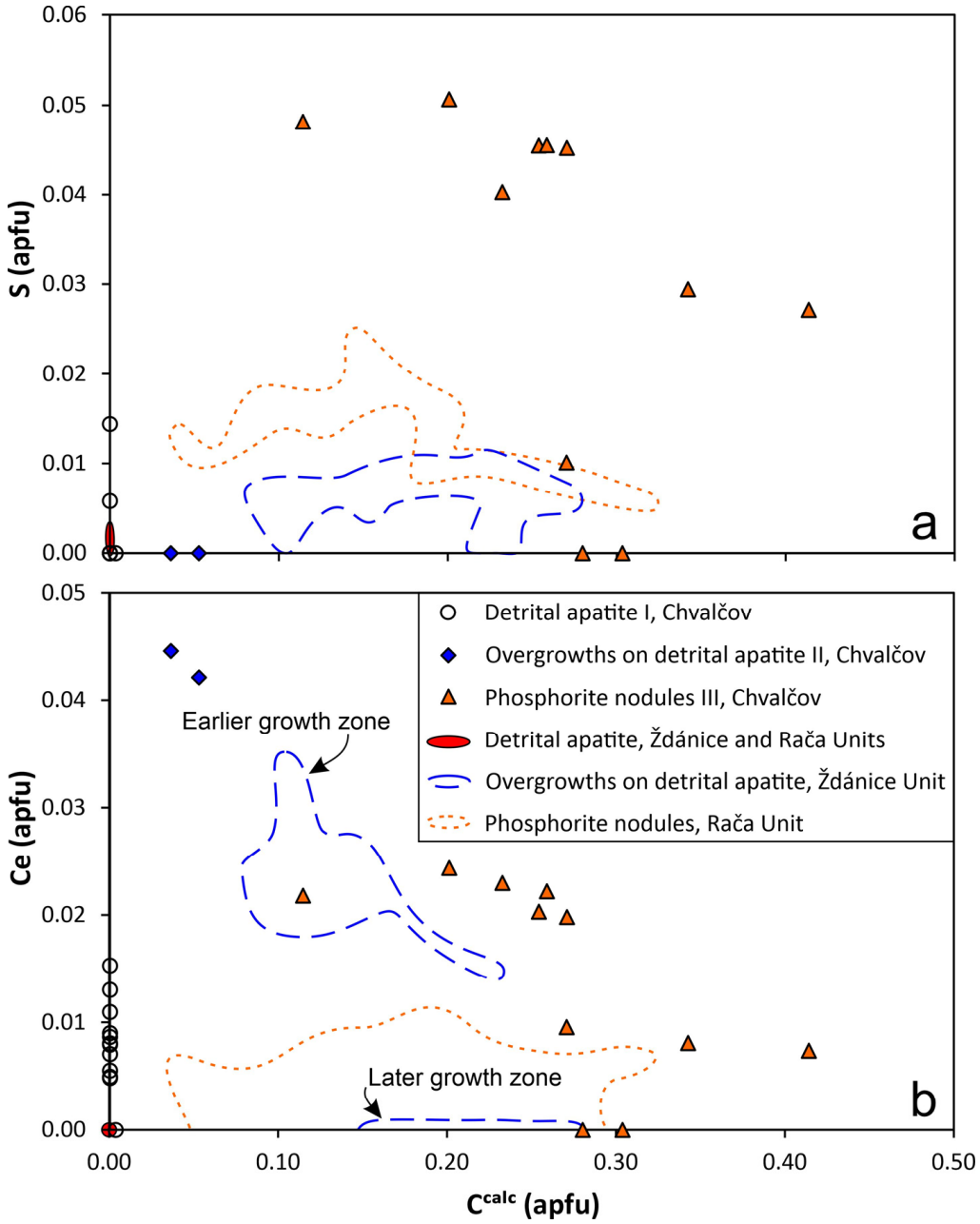

Figure 7. Variations in the chemical composition of apatite from Chvalčov and comparison with published data from neighboring portions of the Flysch Belt. (**a**) Plot C^{calc} vs. S. (**b**) Plot C^{calc} vs. Ce. Comparative data are taken from [14,15,41,42].

5.2. Mechanism of Diagenetic Alteration

The dissolution of detrital mineral grains during diagenesis at deeper burials of siliciclastic sediments is a well-known feature that can have crucial importance for the composition of heavy mineral fractions [43–47]. Depth of burial, temperature, permeability of rocks, chemical composition of fluids, and duration of activity of etching fluids were recognized to be critical factors influencing the intensity of diagenetic dissolution of heavy minerals (e.g., [47]).

The previous works gave evidence for diagenetic alteration of detrital quartz, feldspars, garnet, tourmaline, zircon, monazite, a Fe-Ti mineral, and apatite occurring in sandstones of the Carpathian Flysch Belt [7,9,10,12,14,15]. The intensity of diagenetic alteration can be very high in some cases; ref. [15] estimated the dissolution of about 50% of the original

volume of detrital material. This makes the diagenetic dissolution a relevant reason for explaining the wide variability in content of heavy minerals as well as in mutual proportions of individual heavy minerals in sandstones of the Carpathian Flysch Belt, as found in previous works [3–6]. Although the nature of alterations recognized during our work is qualitatively comparable with those reported by preceding studies [14,15], the new data offer further insights into the nature and relative timing of processes causing the diagenetic alteration of heavy minerals in the studied area. Contrary to previous works, we suggest that the alteration of detrital minerals occurred during at least two geochemically different stages.

5.2.1. Stage I

Stage I took place soon after the deposition of detrital material. Undoubtedly, at this stage, the formation of the T2b TiO_2 phase (in places associated with Fe(-Ti) oxides) at the expense of clasts of a Fe-Ti detrital mineral occurred. This precursor was most probably ilmenite, which was found in large quantities in some less altered sandstones of the Rača Unit (unpublished data of the authors). Although small inclusions of a mineral phase rich in Fe remained preserved in some pseudomorphs (Figure 3d–f), the vast majority of Fe was evidently leached out by the diagenetic fluids in most cases. The mineral phases formed during alteration underwent various degrees of recrystallization in individual clasts, which is indicated by the wide range of observed textures, from unevolved fine-grained compositionally heterogeneous Fe-Ti rich matrix (Figure 3d) up to Fe-depleted well-crystallized newly formed coarse crystals of TiO_2 minerals collecting Ti from a large volume of the former clast (Figure 3k). The latter implies the mobility of Ti in the area defined by the outline of the original detrital grain. However, Ti also migrated out of the area of the clast, which is suggested by the complete dissolution of certain portions of some clasts (Figure 3m–o). Moreover, mobility of Ti on a neighboring-clast scale is clearly indicated by the occurrence of newly crystallized coatings and idiomorphic aggregates of the T3 TiO_2 mineral (brookite), growing over quartz clasts adjacent to altered grains of the Ti mineral (Figure 3p). Because calcite cement grows over these coatings, it is evident that these Stage I alterations had to take place prior to the solidification of the rock, i.e., before the crystallization of calcite cement. A similar style of in situ alteration of detrital ilmenite via pseudorutile up to Fe-poor TiO_2 polymorphs (anatase, brookite, rutile) was reported from a number of sedimentary formations worldwide [48–55].

The increased concentrations of other HFSE elements (Zr, Nb) as well as some other metals (Sc, Cr, V, Al, Y), Si, and P in the newly crystallized TiO_2 phases (both T2a and T2b) imply coeval remobilization of these elements by the same early-diagenetic pore fluids. Although one cannot exclude that some of these elements might be derived from the precursor mineral (i.e., Zr from detrital titanite), we suggest that most of them originated from external sources, namely from the dissolution of other detrital phases (cf. [56]). As was already mentioned above, slight to strong corrosion of zircon, monazite, rutile, tourmaline, garnet, and apatite, as well as alteration of biotite, was documented by this work and previous papers [7,9,10,12,14,15], which could act as sources of the "exotic" elements. Moreover, it is also interesting in this context that the silty-clayey fraction is almost completely missing in these sandstones. Although most fine-grained detritus could be washed out already during sedimentation, it is probable that its remnants could be completely disposed of during early diagenetic processes because of the large reactive surface, allowing for the dissolution of fine particles. This hypothesis can be supported by the lack of clay dispersion in calcite cement or around psammitic clasts. Moreover, a significant replacement of clayey intraclasts by calcite cement was observed in the studied sandstones (Figure 2f).

Stage I was also associated with the dissolution of detrital apatite and monazite (Figures 2f and 5g,h,l), followed by the crystallization of authigenic apatite (Figure 5h). The contemporaneous dissolution of detrital phosphates can explain the increased contents of P in TiO_2 phases formed during alteration of detrital Ti-minerals (T2a, T2b type) as well as in the newly crystallized authigenic TiO_2 phase (T3 type). Similarly, the dissolution of

monazite could be the source of REE, which was incorporated during the crystallization of authigenic rims and veinlets formed by Type II apatite. The REE enrichment in authigenic overgrowths sealing the corroded relics of detrital apatite was observed also in flysch sandstones of the Ždánice Unit [14]. Some REE could also be derived from the dissolution of phosphorite nodules, because (i) these show sometimes some features of corrosion (Figure 2f) and (ii) some of their zones contain elevated amounts of REEs [42] (this study). In any case, the pertinence of apatite dissolution as well as apatite growth to the Stage I episode is clearly suggested by the earlier paragenetic positions of both processes with respect to the formation of calcite cement.

The pore fluids causing the Stage I alterations were likely characterized by a distinct composition. Because they were able to dissolve minerals containing usually poorly mobile HFSE elements (Zr, Nb, Ti), Sc, Y, and REE and transport these elements to small (in case of grain-scale migration) or larger (in case of total dissolution without any signs of re-precipitation in the neighborhood of dissolved mineral grain) distances, we can assume the presence of ligands allowing stabilization of these compounds in aqueous solutions. The REE can be effectively complexed especially by fluoride, hydroxide, carbonate, chloride, sulfate, and/or phosphate anions [57–61]. The mobilization of Ti and Zr could be allowed due to the elevated contents of sulfate and/or fluoride anions in the fluids [62,63]. The pH of the fluid was likely acidic, which further increased the solubility of these elements [64,65] as well as Fe. Lower than neutral pH is also suggested from the dissolution of apatite [64,65] and monazite [64]. Acid environments would also favor the precipitation of anatase and brookite, which are clearly the predominant authigenic TiO_2 polymorphs in the studied sandstone, instead of rutile [66]. The origin of the increased acidity of pore fluids was likely associated with the oxidative degradation of organic matter during this early stage of diagenesis [67,68]. An increased Eh of the fluids is suggested by the presence of iron oxy-hydroxides and a lack of siderite and/or pyrite in alteration assemblages [69,70]. The presence of sulfate, fluoride, and carbonate anions in the pore fluids at this stage is well documented from the composition of authigenic apatite, which contains elevated contents of these compounds.

5.2.2. Stage II

The superimposed Stage II alteration was associated with the dissolution of detrital garnet, feldspars, and quartz. The dissolution propagated not only from the outer surface of the original detrital grains but frequently also along microcracks present in the detrital mineral grains. These microcracks are usually not in situ tectonically induced fissures because they do not continue into neighboring clasts (Figure 5d–f), but they likely represent pre- or syn-sedimentary features. The dissolution process was consistent with the crystallization of calcite cement. It is evidenced by the fact that the extensive dissolution of detrital phases led to the formation of numerous relics of the original phase, which remained mostly in the original position in the realm of former detrital grain (Figure 5d–f). Therefore, the growth of calcite cement in open space produced by dissolution prevented gravitational scattering of the dissolution-derived residual fragments of the original detrital grain. Furthermore, sealing cracks with calcite cement allowed for the frequently observed preservation of some relics of the detrital phase due to isolating them from contact with corrosive fluids. The same nature of dissolution of garnet clasts is also described [14,15] from other sites in the Carpathian Flysch Belt and [33] from Carboniferous freshwater sediments of the Boskovice Graben (Czech Republic). The equilibrium with calcite suggests that corrosive fluids were likely near-neutral to alkaline aqueous solutions at this stage (cf. [71]). As was already mentioned by [14], such diagenetic fluids could potentially be derived from limestone bodies (olistolites or klippen) present in the study area. Alkaline fluids are also very effective in the dissolution of quartz [72–76].

5.3. Further Implications

Our study illustrates substantial changes in the original mineral composition that appeared during the diagenetic alteration of flysch sandstone from the Chvalčov site. Ilmenite, which was probably one of the major components of the original heavy mineral assemblage in this case, was completely altered to porous aggregates of TiO_2 minerals. No relics of the original phase are preserved. A similar fate also experienced titanite, which, however, was likely a minor component of the original heavy mineral assemblage. Because relatively fine-grained polymineral aggregates originated during alteration of both minerals, it is probable that these objects were classified as poorly transparent, unidentifiable grains during routine optical investigation of a heavy mineral concentrate separated from the rock. Structures characterized by substantial dissolution of the precursor matrix and thus now dominated by calcite (Figure 3f–o) would be removed even during gravitational separation of heavy mineral concentrate because of their low average specific gravity. This leads to further loss of information.

In this context, the in situ electron microprobe approach appears as a valuable tool for complex heavy mineral analysis. Its application offers qualitatively different information that is not obtainable from samples processed by the standard methodology used in heavy mineral studies.

6. Conclusions

The in situ electron microprobe study provided important insights into the diagenetic history of detrital material in the Upper Cretaceous-to-Paleogene flysch sandstones of the Rača Unit. Detrital titanite and a Fe-Ti mineral (most probably ilmenite) were almost completely altered to porous aggregates of TiO_2 minerals. Various textural arrangements of alteration products were observed, from unevolved Fe-rich fine-grained matrix to fully recrystallized euhedral crystals of Fe-poor TiO_2 phase grown in space of former detrital grain. In addition, crystallization of the authigenic TiO_2 phase occurred in intergranular spaces of sandstone (i.e., out of the area of former clasts of detrital Ti-minerals). Raman analysis showed that brookite, anatase, and rutile form authigenic TiO_2 phases. The spot electron microprobe analyses yielded occasionally elevated contents of Fe, Nb, Zr, V, Sc, Cr, Al, Y, and/or P in newly formed TiO_2 phases. In addition, the formation of REE- and Y-enriched authigenic apatite around detrital apatite was rarely found. Our observations suggest the mobility of HFSE and REE during the early diagenetic history of rock, which occurred prior to the formation of calcite cement. This was probably allowed due to the presence of REE- and HFSE-complexing ligands like sulfate and/or fluoride anions, possibly in combination with the acidic pH of the pore fluids. The later formation of calcite cement was associated with the partial dissolution of detrital garnet, feldspars, and quartz. The chemical composition of garnet and apatite is comparable to that of adjacent parts of the Carpathian Flysch Belt. The present study illustrates the usefulness of an in situ electron microprobe study for the complex evaluation of processes influencing the heavy mineral assemblages in diagenetically altered sedimentary rocks. Our observations yield further evidence that diagenetic processes can deeply alter the composition of the original heavy mineral assemblage and change the quantitative proportions of individual minerals, even in the case of major components.

Supplementary Materials: The following supporting information can be downloaded at: https://www.mdpi.com/article/10.3390/min14010001/s1. Table S1: A complete dataset of electron-microprobe analyses of minerals Chvalcov-supplementary.xlsx.

Author Contributions: Conceptualization, Z.D. and M.K.K.; investigation, Z.D., M.K.K., J.U. and J.S.; writing—original draft preparation, Z.D. and M.K.K.; writing—review and editing, Z.D., M.K.K., J.U. and J.S. All authors have read and agreed to the published version of the manuscript.

Funding: This research was funded by the Ministry of Culture of the Czech Republic (DKRVO 2019–2023/1.II.e., 00023272) for Z.D., J.U. and J.S.

Data Availability Statement: All data are contained in this work and the Supplementary Materials.

Acknowledgments: This work was supported by the Ministry of Culture of the Czech Republic (DKRVO 2019-2023/1.II.e., 00023272) to Z.D., J.U., and J.S. The constructive reviews by two anonymous referees are highly appreciated.

Conflicts of Interest: The authors declare no conflict of interest. The funder had no role in the design of this study, in the collection, analysis, or interpretation of data, in the writing of this manuscript, or in the decision to publish these results.

References

1. Otava, J.; Krejčí, O.; Sulovský, P. First results of electron microprobe analyses of detrital garnets from the Rača Unit of the Magura Group. *Geol. Výzk. Mor. Slez. Roce 1996* **1997**, *4*, 39–42. (In Czech)
2. Otava, J.; Krejčí, O.; Sulovský, P. The results of study of detrital garnets from the Cretaceous sediments Rača Unit of the Magura Group (Outer Carpathians). *Geol. Výzk. Mor. Slez. Roce 1997* **1998**, *5*, 29–31. (In Czech)
3. Gilíková, H.; Otava, J.; Stráník, Z. Petrological characteristics of sediments of the Magura Flysch at the map-sheet Holešov. *Geol. Výzk. Mor. Slez. Roce 2001* **2002**, *9*, 26–29. (In Czech)
4. Kropáč, K.; Dolníček, Z.; Janál, J. Heavy minerals in the building material of „Obřany" ruin and in surrounding rocks (Hostýn Hills). *Geol. Výzk. Mor. Slez. Roce 2003* **2004**, *11*, 91–93. (In Czech)
5. Oszczypko, N.; Salata, D. Provenance analyses of the Late Cretaceous—Paleocene deposits of the Magura basin (Polish Western Carpathians)—Evidence from a study of the heavy minerals. *Acta Geol. Polon.* **2005**, *55*, 237–267.
6. Stráník, Z.; Hrouda, F.; Otava, J.; Gilíková, H.; Švábenická, L. The Upper Oligocene-Lower Miocene Krosno lithofacies in the Carpathian Flysch Belt (Czech Republic): Sedimentology, provenance and magnetic fabrics. *Geol. Carpath.* **2007**, *58*, 321–332.
7. Bónová, K.; Bóna, J.; Kováčik, M.; Laurinc, D. Heavy minerals from sedimentary rocks of the Malcov Formation and their palaeogeographic implications for evolution of the Magura Basin (Western Carpathians, Slovakia) during the Late Eocene–Late Oligocene. *Geol. Quart.* **2016**, *60*, 675–694. [CrossRef]
8. Bónová, K.; Spišiak, J.; Bóna, J.; Kováčik, M. Chromian spinels from the Magura Unit (Western Carpathians, Eastern Slovakia)—Their petrogenetic and palaeogeographic implications. *Geol. Quart.* **2017**, *61*, 3–17. [CrossRef]
9. Bónová, K.; Bóna, J.; Kováčik, M.; Mikuš, T. Heavy minerals and exotic pebbles from the Eocene flysch deposits of the Magura Nappe (Outer Western Carpathians, Eastern Slovakia): Their composition and implications on the provenance. *Turk. J. Earth Sci.* **2018**, *27*, 64–88. [CrossRef]
10. Bónová, K.; Mikuš, T.; Bóna, J. Is Cr-spinel geochemistry enough for solving the provenance dilemma? Case study from the Palaeogene sandstones of the Western Carpathians (Eastern Slovakia). *Minerals* **2018**, *8*, 543. [CrossRef]
11. Bellová, S.; Aubrecht, R.; Mikuš, T. First results of systematic provenance analysis of the heavy mineral assemblages from the Albian to Cenomanian exotic flysches of the Klape Unit, Tatricum, Fatricum and some adjacent units. *Acta Geol. Slov.* **2018**, *10*, 45–64.
12. Bónová, K.; Bóna, J.; Pańczyk, M.; Kováčik, M.; Mikuš, T.; Laurinc, D. Origin of deep-sea clastics of the Magura Basin (Eocene Makovica sandstones in the Outer Western Carpathians) with constraints of framework petrography, heavy mineral analysis and zircon geochronology. *Palaeogeogr. Palaeoclimat. Palaeoecol.* **2019**, *514*, 768–784. [CrossRef]
13. Aubrecht, R.; Bačík, P.; Mikuš, T.; Bellová, S. Detritic tourmalines with complex zonation in the Cretaceous exotic flysches of the Western Carpathians: Where did they come from? *Lithos* **2020**, *362–363*, 105443. [CrossRef]
14. Dolníček, Z.; Krejčí Kotlánová, M.; Koutňák, R. Influence of diagenetic processes on assemblage of heavy minerals in sandstones from the locality Slivotín (Ždánice Unit, Flysch Belt of the Outer Western Carpathians, Czech Republic). *Bull. Mineral. Petrolog.* **2021**, *29*, 27–40. (In Czech) [CrossRef]
15. Dolníček, Z.; Krejčí Kotlánová, M. A pronounced diagenetic alteration of heavy minerals in sandstones from the locality Lukoveček (Rača Unit, Flysch Belt of the Outer Western Carpathians, Czech Republic). *Acta Mus. Morav. Sci. Geol.* **2022**, *107*, 53–71. (In Czech)
16. Plašienka, D.; Grecula, P.; Putiš, M.; Kováč, M.; Hovorka, D. Evolution and structure of the Western Carpathians: An overview. In *Geological Evolution of the Western Carpathians*; Grecula, P., Hovorka, D., Putiš, M., Eds.; Mineralia Slovaca: Bratislava, Slovakia, 1997; pp. 1–24.
17. Stráník, Z. Flysch Belt. In *Geology of Outer Western Carpathians and South-East Margin of West-European Platform in the Czech Republic*; Stráník, Z., Bubík, M., Gilíková, H., Tomanová Petrová, P., Eds.; Czech Geological Survey: Prague, Czech Republic, 2021; pp. 95–234. (In Czech)
18. Picha, F.J.; Stráník, Z.; Krejčí, O. Geology and hydrocarbon resources of the Outer Western Carpathians and their foreland, Czech Republic. In *The Carpathians and Their Foreland: Geology and Hydrocarbon Resources*; Golonka, J., Picha, F.J., Eds.; American Association of Petroleum Geologists: Tulsa, OK, USA, 2006; Volume 84, pp. 49–175.

19. Gebhardt, H. Lower Miocene olistostromes and giant-olistoliths: A new interpretation of the Eocene Waschberg Limestone occurrences and consequences for the structural composition of the southern Waschberg–Ždánice Unit in Lower Austria. *Geol. Carpath.* **2021**, *72*, 48–67. [CrossRef]
20. Botor, D.; Dunkl, I.; Rauch-Włodarska, M.; von Eynatten, H. Attempt to dating of accretion in the West Carpathian Flysch Belt: Apatite fission track thermochronology of tuff layers. *Geolines* **2006**, *20*, 21–23.
21. Jarmolowicz-Szulc, K.; Karwowski, L.; Marynowski, L. Fluid circulation and formation of minerals and bitumens in the sedimentary rocks of the Outer Carpathians—Based on studies on the quartz–calcite–organic matter association. *Mar. Petrol. Geol.* **2012**, *32*, 138–158. [CrossRef]
22. Vlasáková, J.; Kropáč, K. Hydrothermal mineralization in rocks of the Soláň Formation in the western part of Chřiby Hills. *Geol. Výzk. Mor. Slez.* **2016**, *23*, 39–44. (In Czech)
23. Hurai, V.; Kihle, J.; Kotulová, J.; Marko, F.; Świerczewska, A. Origin of methane in quartz crystals from the Tertiary accretionary wedge and fore-arc basin of the Western Carpathians. *Appl. Geochem.* **2002**, *17*, 1259–1271. [CrossRef]
24. Dolníček, Z.; Kropáč, K.; Janíčková, K.; Urubek, T. Diagenetic source of fluids causing the hydrothermal alteration of teschenites in the Silesian Unit, Outer Western Carpathians, Czech Republic: Petroleum-bearing vein mineralization from the Stříbrník site. *Mar. Petrol. Geol.* **2012**, *37*, 27–40. [CrossRef]
25. Pesl, V.; Čekan, V.; Eliáš, M.; Hanzlíková, E.; Jetel, J.; Peslová, H.; Růžička, M. *Explanations to Geological Map 1:25000 Sheet 25-143 Bystřice pod Hostýnem*; MS, Czech Geological Survey: Prague, Czech Republic, 1981; 74p. (In Czech)
26. Bubík, M. Deep-water agglutinated foraminifera biofacies in the Outer Flysch Belt of the Carpathians. *Geol. Výzk. Mor. Slez. v r.* **1995**, *1996*, 48–50. (In Czech)
27. Pouchou, J.L.; Pichoir, F. "PAP" (φρZ) procedure for improved quantitative microanalysis. In *Microbeam Analysis*; Armstrong, J.T., Ed.; San Francisco Press: San Francisco, CA, USA, 1985; pp. 104–106.
28. Marfil, R.; Rossi, C.; Lozano, R.P.; Permanyer, A.; Ramseyer, K. Quartz cementation in Cretaceous and Jurassic reservoir sandstones from the Salam oil field, Western Desert, Egypt: Constraints on temperature and timing of formation of fluid inclusions. In *Quartz Cementation in Sandstones*; Worden, R., Morad, S., Eds.; Blackwell Science: Oxford, UK, 2000; pp. 163–182.
29. Shogenova, A.; Kleesment, A.; Hirt, A.; Pirrus, E.; Kallaste, T.; Shogenov, K.; Vaher, R. Composition and properties of the iron hydroxides-cemented lenses in Estonian sandstone of Middle Devonian age. *Stud. Geophys. Geodaet.* **2009**, *53*, 111–131. [CrossRef]
30. Worden, R.H.; Morrall, G.T.; Kelly, S.; Mc Ardle, P.; Barshep, D.V. A renewed look at calcite cement in marine-deltaic sandstones: The Brent Reservoir, Heather Field, northern North Sea, UK. *Geol. Soc. London Spec. Publ.* **2019**, *484*, 305–335. [CrossRef]
31. Bastin, E.S. *Interpretation of Ore Textures*; Geological Society of America: Boulder, CO, USA, 1950; Volume 45.
32. Kutina, J. Genetische Diskussion der Makrotexturen bei der geochemischen Untersuchung des Adalbert-Hauptganges in Příbram. *Chem. Erde* **1955**, *17*, 241–323.
33. Hršelová, P.; Houzar, S.; Štelcl, J. Corroded garnets in the association of heavy minerals of Balinka conglomerates: Their morphology and chemical composition (Upper Carboniferous, Boskovice Basin). *Acta Mus. Morav. Sci. Geol.* **2021**, *106*, 35–50. (In Czech)
34. Bónová, K.; Jafarzadeh, M.; Bóna, J. Depositional history of the Devonian Ilanqareh and Padeha Formations in Azarbaijan Province and Eastern Alborz (Iran): Constraints from heavy-mineral microtextures. *Acta Geol. Slov.* **2021**, *13*, 13–26.
35. Stormer, J.C., Jr.; Pierson, M.J.; Tacker, R.C. Variation of F and Cl X-ray intensity due to anisotropic diffusion of apatite during electron microprobe analysis. *Am. Mineral.* **1993**, *78*, 641–648.
36. Morton, A.; Yaxley, G. Detrital apatite geochemistry and its application in provenance studies. In *Sedimentary Provenance and Petrogenesis: Perspectives from Petrography and Geochemistry*; Arribas, J., Johnsson, M.J., Critelli, S., Eds.; Geological Society of America: Boulder, CO, USA, 2007; Volume 420, pp. 319–344.
37. Matýsek, D.; Skupien, P. Phosphorite concretions in the Upper Cretaceous of the Silesian Unit. *Geol. Výzk. Mor. Slez. Roce 2004* **2005**, *12*, 34–36. (In Czech)
38. Slansky, M. *Geology of Sedimentary Phosphates*; North Oxford Academic: London, UK, 1986.
39. Froelich, P.N.; Arthur, M.A.; Burnett, W.C.; Deakin, M.; Hensley, V.; Jahnke, R.; Kaul, L.; Kim, K.-H.; Roe, K.; Soutar, A.; et al. Early diagenesis of organic matter in Peru continental margin sediments: Phosphorite precipitation. *Mar. Geol.* **1988**, *80*, 309–343. [CrossRef]
40. Stalder, M.; Rozendaal, A. Apatite nodules as an indicator of depositional environment and ore genesis for the Mesoproterozoic Broken Hill-type Gamsberg Zn–Pb deposit, Namaqua Province, South Africa. *Miner. Depos.* **2004**, *39*, 189–203. [CrossRef]
41. Dolníček, Z.; Kandrnál, L.; Ulmanová, J.; Vratislavská, E.; Hojač, P. Historical mining of pelosiderites at the locality Koryčanská cesta near Moravany, southern part of the Chřiby Mts. *Bull. Mineral. Petrolog.* **2019**, *27*, 304–316. (In Czech)
42. Dolníček, Z.; Kandrnál, L.; Ulmanová, J.; Vratislavská, E.; Hojač, P. Mineralogy of a rhodochrosite-bearing phosphorite concretion from the locality Tabarky, northern part of the Chřiby Mts. *Bull. Mineral. Petrolog.* **2020**, *28*, 35–43. (In Czech) [CrossRef]
43. Morton, A.C. *Heavy Minerals*; Springer: Berlin/Heidelberg, Germany, 1978.
44. Morton, A.C. Influences of provenance and diagenesis on detrital garnet suites in the Paleocene Forties Sandstone, Central North Sea. *J. Sediment. Res.* **1987**, *57*, 1027–1032.
45. Smale, D.; Morton, A.C. Heavy mineral suites of core samples from the McKee Formation (Eocene-Lower Oligocene), Taranaki: Implications for provenance and diagenesis. *N. Zeal. J. Geol. Geophys.* **1988**, *30*, 299–306. [CrossRef]

46. Milliken, K.L.; Mack, L.E. Subsurface dissolution of heavy minerals: Frio Formation sandstones of the ancestral Rio Grande Province, South Texas. *Sediment. Geol.* **1990**, *68*, 187–199. [CrossRef]
47. Morton, A.C.; Hallsworth, C.R. Stability of detrital heavy minerals during burial diagenesis. In *Heavy Minerals in Use*; Developments in Sedimentology; Mange, M.A., Wright, D.T., Eds.; Elsevier: Amsterdam, The Netherlands, 2007; Volume 58, pp. 215–245.
48. Austin, S.R. Ilmenite, magnetite, and feldspar alteration under reducing conditions. *Econ. Geol.* **1960**, *55*, 1758–1759. [CrossRef]
49. Morad, S.; Adin Aldahan, A. Authigenesis of titanium minerals in two Proterozoic sedimentary rocks from southern and central Sweden. *J. Sediment. Res.* **1982**, *52*, 1295–1305.
50. Morad, S.; Adin Aldahan, A. Alteration of detrital Fe-Ti oxides in sedimentary rocks. *Geol. Soc. Am. Bull.* **1986**, *96*, 567–578. [CrossRef]
51. Mücke, A.; Chaudhuri, J.N.B. The continuous alteration of ilmenite through pseudorutile to leucoxene. *Ore Geol. Rev.* **1991**, *6*, 25–44. [CrossRef]
52. Weibel, R. Alteration of detrital Fe-Ti oxides in Miocene fluvial deposits, central Jutland, Denmark. *Bull. Geol. Soc. Denmark* **2003**, *50*, 141–208. [CrossRef]
53. Pe-Piper, G.; Piper, D.J.W.; Dolansky, L. Alteration of ilmenite in the Cretaceous sandstones of Nova Scotia, southeastern Canada. *Clays Clay Miner.* **2005**, *53*, 490–510. [CrossRef]
54. Pownceby, M.I. Alteration and associated impurity element enrichment in detrital ilmenites from the Murray Basin, southeast Australia: A product of multistage alteration. *Austral. J. Earth Sci.* **2010**, *57*, 243–258. [CrossRef]
55. Nallusamy, B.; Babu, S.; Suresh Babu, D.S. Heavy mineral distribution and characterisation of ilmenite of Kayamkulam—Thothapally Barrier Island, southwest coast of India. *J. Geol. Soc. Ind.* **2013**, *81*, 129–140. [CrossRef]
56. Frost, M.; Grey, I.; Harrowfield, I.; Mason, K. The dependence of alumina and silica contents on the extent of alteration of weathered ilmenites from Western Australia. *Min. Mag.* **1983**, *47*, 201–208. [CrossRef]
57. Bau, M.; Möller, P. Rare earth element fractionation in metamorphogenic hydrothermal calcite, magnesite and siderite. *Mineral. Petrol.* **1992**, *45*, 231–246. [CrossRef]
58. Williams-Jones, A.E.; Migdisov, A.A.; Samson, I.A. Hydrothermal mobilisation of the rare earth elements—A tale of "ceria" and "yttria". *Elements* **2012**, *8*, 355–360. [CrossRef]
59. Migdisov, A.A.; Williams-Jones, A.E. Hydrothermal transport and deposition of the rare earth elements by fluorine-bearing aqueous liquids. *Miner. Depos.* **2014**, *49*, 987–997. [CrossRef]
60. Migdisov, A.; Williams-Jones, A.E.; Brugger, J.; Caporuscio, F.A. Hydrothermal transport, deposition, and fractionation of the REE: Experimental data and thermodynamic calculations. *Chem. Geol.* **2016**, *439*, 13–42. [CrossRef]
61. Migdisov, A.; Guo, X.; Nisbet, H.; Xu, H.; Williams-Jones, A.E. Fractionation of REE, U, and Th in natural ore-forming hydrothermal systems: Thermodynamic modeling. *J. Chem. Thermodyn.* **2019**, *128*, 305–319. [CrossRef]
62. Rubin, J.N.; Henry, C.D.; Price, J.G. The mobility of zirconium and other immobile elements during hydrothermal alteration. *Chem. Geol.* **1993**, *110*, 29–47. [CrossRef]
63. Jiang, S.-Y.; Wang, R.-C.; Xu, X.-S.; Zhao, K.-D. Mobility of high field strength elements (HFSE) in magmatic-, metamorphic-, and submarine-hydrothermal systems. *Phys. Chem. Earth A/B/C* **2005**, *30*, 1020–1029. [CrossRef]
64. Ayers, J.C.; Watson, B.E. Solubility of apatite, monazite, zircon, and rutile in supercritical aqueous fluids with implications for subduction zone geochemistry. *Phil. Trans. R. Soc. Lond. A Phys. Eng. Sci.* **1991**, *335*, 365–375.
65. Guidry, M.W.; Mackenzie, F.T. Experimental study of igneous and sedimentary apatite dissolution: Control of pH, distance from equilibrium, and temperature on dissolution rates. *Geochim. Cosmochim. Acta* **2003**, *67*, 2949–2963. [CrossRef]
66. Cassaignon, S.; Koelsch, M.; Jolivet, J.P. Selective synthesis of brookite, anatase and rutile nanoparticles: Thermolysis of $TiCl_4$ in aqueous nitric acid. *J. Mater. Sci.* **2007**, *42*, 6689–6695. [CrossRef]
67. Curtis, C. Mineralogical consequence of organic matter degradation in sediments: Inorganic/organic diagenesis. In *Marine Clastic Sedimentology—Concepts and Case Studies*; Legget, J.K., Zuffa, G.G., Eds.; Springer: Dordrecht, The Netherlands, 1987; pp. 108–123.
68. Sanders, D. Syndepositional dissolution of calcium carbonate in neritic carbonate environments: Geological recognition, processes, potential significance. *J. Afr. Earth Sci.* **2003**, *36*, 99–134. [CrossRef]
69. Carrol, D. Ilmenite alteration under reducing conditions in unconsolidated sediments. *Econ. Geol.* **1960**, *55*, 618–619. [CrossRef]
70. Dill, H.G. Authigenic heavy minerals a clue to unravel supergene and hypogene alteration of marine and continental sediments of Triassic to Cretaceous age (SE Germany). *Sediment. Geol.* **2010**, *228*, 61–76. [CrossRef]
71. Nickel, E. Experimental dissolution of light and heavy minerals in comparison with weathering and intrastratal solution. *Contr. Sedimentol.* **1973**, *1*, 1–68.
72. Fiala, V.; Čadek, J. Hydrothermal alterations at the deposit Okrouhlá Radouň. *Sborn. Geol. Věd. Ložisk. Geol. Mineral.* **1981**, *22*, 159–199. (In Czech)
73. Dolníček, Z.; René, M.; Hermannová, S.; Prochaska, W. Origin of the Okrouhlá Radouň episyenite-hosted uranium deposit, Bohemian Massif, Czech Republic: Fluid inclusion and stable isotope constraints. *Miner. Depos.* **2014**, *49*, 409–425. [CrossRef]
74. Li, S.; Tian, J.; Lin, X.; Zuo, Y.; Kang, H.; Yang, D. Effect of alkaline diagenesis on sandstone reservoir quality: Insights from the Lower Cretaceous Erlian Basin, China. *Energy Explor. Exploit.* **2020**, *38*, 434–453. [CrossRef]

75. Wang, Y.; Qiu, L.; Yang, Y.; Xu, W.; Khan, D.; Qiao, Y. Coupling between tectonic activity and diagenetic evolution of a clastic buried hill—A case study from Gubei low buried hill in Jiyang Depression of Bohai Bay Basin. *Arab. J. Geosci.* **2021**, *14*, 194. [CrossRef]
76. Sejkora, J.; Dolníček, Z.; Škácha, P.; Ulmanová, J.; Vrtiška, L. Unusual mineralization with willemite from the area of the central part of the Příbram uranium and base-metal district (Czech Republic). *Bull. Mineral. Petrolog.* **2022**, *30*, 224–242. (In Czech) [CrossRef]

Disclaimer/Publisher's Note: The statements, opinions and data contained in all publications are solely those of the individual author(s) and contributor(s) and not of MDPI and/or the editor(s). MDPI and/or the editor(s) disclaim responsibility for any injury to people or property resulting from any ideas, methods, instructions or products referred to in the content.